

## **Tensile Testing of Aged Flexible Unidirectional Composite Laminates for Body Armor**

Amy Engelbrecht-Wiggans<sup>1, 2</sup>, Faraz Burni<sup>1, 3</sup>, Ajay Krishnamurthy<sup>1, 2</sup>, Amanda L. Forster\*<sup>1</sup>

<sup>1</sup>Material Measurement Laboratory, National Institute of Standards and Technology, Gaithersburg, MD, USA

<sup>2</sup>Theiss Research, La Jolla, CA, USA

<sup>3</sup>Chemical and Biomolecular Engineering Department, University of Maryland, College Park, MD, USA

Amy Engelbrecht-Wiggans

e-mail address: aee@nist.gov, aee52@cornell.edu

Telephone number: (301) 975-8580

ORCID: 0000-0002-5292-7970

Mailing address:

National Institute of Standards and Technology

Gaithersburg, MD 20899

mailstop 8102

Amanda L. Forster

e-mail address: amanda.forster@nist.gov

Telephone number: (301) 975-5632

ORCID: 0000-0001-7397-4429

Mailing address:

National Institute of Standards and Technology

Gaithersburg, MD 20899

mailstop 8102

Faraz Burni

e-mail address: faraz.burni@nist.gov

ORCID: 0000-0003-3262-0653

Ajay Krishnamurthy

ORCID: 0000-0001-8608-3721

e-mail address: ajay.krishnamurthy@nist.gov

Keywords: Composite laminate, flexible composite, strip tensile testing, body armor, aramid, hydrothermal ageing

## Abstract

Flexible Unidirectional (UD) composite laminates are commonly being used for ballistic-resistant body armor. These laminates comprise UD layers, each constructed by laminating thin layers of high-performance fibers held in place using very low modulus binder resins, with the fibers in each layer oriented parallel to each other. As these materials are used in body armor, it is important to investigate their long-term reliability, particularly with regards to exposure to temperature and humidity as these are known causes of degradation in other commonly used body armor materials. This work investigates the tensile behavior of a poly(p-phenylene terephthalamide), or PPTA flexible UD laminate aged for up to 150 d at accelerated conditions of 70 °C and 76 % relative humidity (RH). Tests were performed at three different crosshead displacement rates and three different gauge lengths. The effect of ageing on the mechanical properties of the material resulted in less than 10 % degradation in tensile strength, with a more significant reduction in longer specimens when tested at slower rates.

## Introduction

Body armor has, to date, saved over 3100 law enforcement officers' lives [1]. To investigate the long-term safety, dependability, and effectiveness of body armor, it is critical to understand the stability of the materials from which armor is made. The investigation of a field failure of a body armor made from poly(p-phenylene-2,6-benzobisoxazole), or PBO, in 2003, resulted in the formation of a research program at the National Institute of Standards and Technology (NIST) that focuses on the stability of such high-strength fibers. For example, PBO was found to degrade rapidly with exposure to humidity [2, 3], leading to major revisions in the National Institute of Justice's (NIJ's) body armor standard [4]. Since the release of this revised standard, work has continued at NIST to examine the mechanisms of ageing in other commonly used fibers such as ultra-high-molar-mass polyethylene (UHMMPE) [5, 6] and poly(p-phenylene terephthalamide), or PPTA, commonly known as aramid [7].

While most body armor is made from woven fabrics, some newer body armor is made from flexible composite laminates, which feel similar to woven fabrics but lack the woven construction. These laminates are made up of thin layers (<0.05 mm) of unidirectional (UD) continuous fibers, where the fibers in consecutive layers are aligned perpendicular to each other, as depicted in Figure 1. These laminates are typically constructed from layers of aligned PPTA or UHMMPE fibers held in place with a small amount (20 % or less by mass [8]) of a binder resin. Flexible UD composite laminates offer several advantages over woven material, in that they avoid the strength loss typically caused by weaving, and also utilize smaller diameter fibers to provide a similar performance to woven fabrics but at a lower weight.

The term "unidirectional" may have several different definitions, depending on the end-use application of the final product. For example, in aerospace composite applications, layers may be hundreds of fibers thick with a matrix volume fraction between 35 % and 50 % [9]. In contrast, in body armor applications, unidirectional generally refers to a layup of alternating orthogonal layers, where each layer has a thickness of less than 10 fibers. In addition, the matrix volume fraction is comparatively very low due to the near-hexagonal

packing arrangement of the fibers [8]. For the purposes of this work, the intended application of the material is for body armor, and full details of the material are given in the Experimental section.

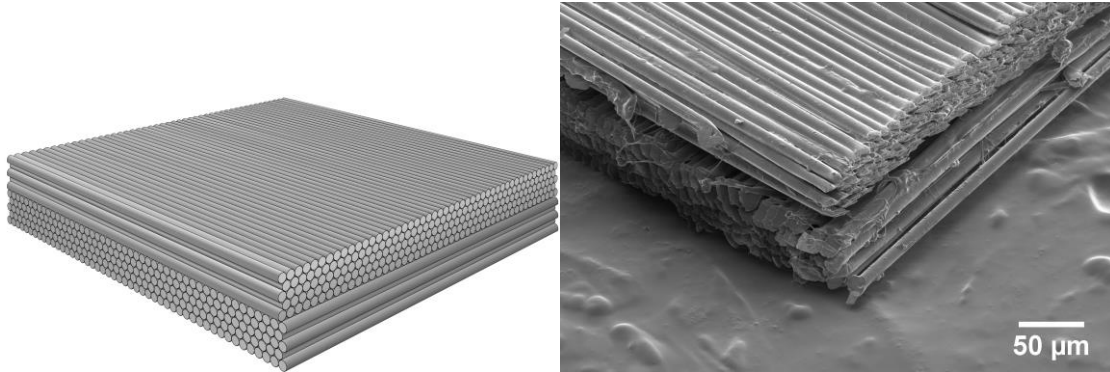


**Figure 1** Schematic representation (left) of the UD laminate, showing the hexagonal packing and the five fiber thick perpendicular layers, and a micrograph (right) showing the structure of the actual material.

PPTA is a condensation polymer and is susceptible to degradation [10, 11] by chain scission through a hydrolysis reaction that attacks the amide linkage between phenylene rings; this hydrolysis is generally expected to be catalyzed by an acid or base [12]. PPTA has been found to physically and chemically degrade with exposure to environments of elevated temperature, humidity, light, pH, or some combination thereof [3, 10, 11, 13–20]. The susceptibility of this material to degradation by ultraviolet (UV) light is well-known, and armor packages are designed to protect the PPTA from exposure to UV light [21]. The effects of exposing PPTA to elevated temperature and relative humidity (RH) have been documented by [7, 10, 11, 14]. These studies typically investigate temperatures in excess of 100 °C for relatively short times, and only one study, [7], uses timeframes and conditions likely to be seen in body armor. From these studies it is apparent that PPTA is susceptible to degradation with exposure to high temperatures and humidity but degrades very slowly under typical use conditions for body armor.

In contrast to the PPTA fibers, only preliminary research has been performed to characterize the ageing of the binder resins used in these UD laminates. Furthermore, the effect of binder ageing on the ballistic performance of the UD laminate is unclear as the impact force is carried mainly by the fibers. Yet during the development of the conditioning protocol used in NIJ Standard-0101.06, the aged UD laminates showed visual signs of delamination and reductions in  $V_{50}$  [22] after ageing, where  $V_{50}$  is the velocity at which half of the projectiles are expected to penetrate the armor [23]. These results demonstrate the need for a thorough understanding of the UD laminate’s material properties with ageing in order to evaluate the material’s long-term structural performance.

Very little research [24] has been carried out to evaluate the tensile strength of flexible UD composite laminates. Most UD composite tensile testing is on rigid UD composites, as in [25–32]. While the flexible laminates can be built up and hot pressed into a rigid composite, this is not done in soft body armor, where this material is used. Hot pressing was thus not explored, as it is not expected to give representative results for the flexible material as it is

used in body armor. Since the exact role of the binder is not fully understood, it is necessary to test the entire composite as a whole to comprehensively determine the effects of ageing.

This study focuses on the tensile strength of an aramid flexible UD laminate under one set of environmental ageing conditions. The tensile strength was chosen as a relevant metric because it can be related to the material's  $V_{50}$  through research by Cunniff [33] and by Phoenix and Porwal [34].

## Experimental

The flexible UD composite laminate used in this study consisted of two layers, each layer having a thickness of approximately 5 PPTA fibers, each with an approximate diameter of 11  $\mu\text{m}$ , all held in place with a very low modulus binder resin. The laminate was aged in an environmental chamber at 70 °C and 76 % RH and extracted at five different time intervals: approximately 30 d, 60 d, 90 d, 120 d and 150 d. This particular ageing condition was chosen based on prior studies of PPTA to accelerate the ageing process as much as possible without inducing new forms of degradation, such as combustion, and also because there are prior studies of PPTA fibers at this specific ageing condition [7]. The environmental chamber provided control to  $\pm 1$  °C and  $\pm 5$  % RH.

The unaged and aged laminates were cut into 30 mm wide specimens of various lengths (100 mm, 300 mm and 900 mm gauge lengths) and tensile tested at three different crosshead displacement rates (1 mm/min, 10 mm/min, and 100 mm/min). Cutting was performed on a self-healing cutting mat using a medical scalpel and a straight edge. Care was taken to align the specimens with the fiber direction. Unless otherwise stated, specimens were cut with their length nominally perpendicular to the axis of the material roll, i.e. such that they would be along the warp fibers if the material were woven. After cutting, the specimens were then tensile tested using capstan grips in a screw driven universal load frame equipped with a 5 kN load cell. A non-contacting video extensometer was used to measure strain at three different locations along each specimen's width, and these three strain values were averaged to determine the failure strain. Further details, and rationales, on the specimen ageing, cutting and testing procedure are described in [35]. Scanning Electron Microscopy (SEM) imaging of the unaged fiber laminate was carried out after depositing a nominal (3 nm – 5 nm) Au/Pd coating on a small laminate cross-section (less than 0.5 mm by 0.5 mm by 1 mm). The imaging parameters were kept identical to previous studies described in [34].

For convenience, the terms 'warp' and 'weft' will be used to describe specimen orientation with regards to the original roll of material, even though this material is not woven and thus does not technically have a 'warp' or 'weft.' The 'warp' direction is that perpendicular to the axis of the cylindrically-shaped bolt on which the material is rolled, while the 'weft' direction is parallel to the bolt's axis. Clarifying figures to indicate specimen orientation and warp and weft terms are provided in [35].

For the purposes of this paper, the stress values reported are the load values divided by the total cross-sectional area. The thickness was determined by measurements of the bulk unaged material at 18 locations throughout the roll using an electronic micrometer with a friction thimble (resolution of 0.001 mm and precision of 0.002 mm). The average thickness was 0.106 mm with a standard deviation of 0.002 mm. For comparison, the

thickness was also measured at five locations from SEM micrographs. For each micrograph an algorithm was used to calculate the average distances between the top and bottom surfaces over 0.75 mm. An average thickness of 0.109 mm with a standard deviation of 0.002 mm was determined using this method. Figure 2 shows a typical SEM micrograph of the cross-section, with a single thickness measurement marked. For calculating the cross-sectional area, the 0.106 mm value for thickness was used along with the nominal specimen cutting width.

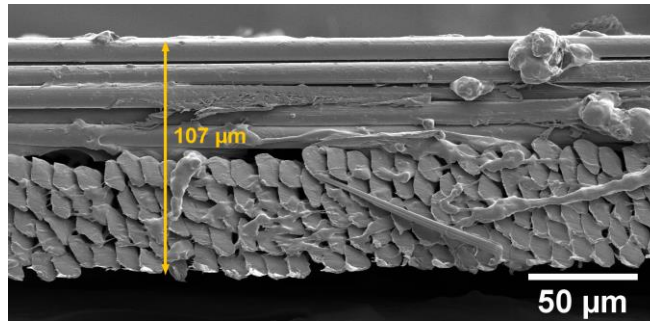


**Figure 2** A scanning electron microscope (SEM) micrograph of a typical cross-section of the UD laminate.

If the fiber volume fraction is known, then the composite stress can be related to the fiber stress through the rule of mixtures. For a composite with such a large difference in modulus between the binder matrix and the fibers, the fiber stress can be approximated by dividing the load by the cross-sectional area of fibers parallel to the direction of the applied load. Fiber volume fraction was estimated by the following method, first the number of fibers in given SEM micrograph (such as Figure 2) were counted for a fixed rectangular area, then the cross-sectional area of individual fibers were determined by mapping the visible fiber cross-section, then the total area occupied by the fiber was computed and used to determine the fiber volume fraction. Specific information on these calculations can be found in the supplemental information. Based on this method, the overall estimate of the fiber volume fraction for this UD laminate is approximately 78%, with a standard deviation of approximately 3 % based on fibers per unit area measurements from four different micrographs and cross-sectional areas from seven different fibers.

## Modeling

### Weibull modeling

The failure process for fiber bundles, both with and without a matrix, has been a subject of research since the 1930's. Weibull [36] applied a 'weakest link' approach to describe the strength of a single fiber, in which the fiber segment with the lowest individual strength fails first, causing overall fiber failure. Over the years, the Weibull distribution has become commonly used to describe both fiber and composite strength [37]. Three common assumptions for how fiber failure is handled in a composite are global load sharing, equal load sharing, and local load sharing [37]. Global load sharing assumes that when a fiber fails it is fully unloaded and the remaining fibers all share the full load equally, as in fiber bundles without a matrix (or yarns) [38]. Equal load sharing assumes that a failed fiber only unloads for a short distance, but then all the remaining fibers in that length share load

[39]. Local load sharing assumes that only the fibers near a break are overloaded, resulting in local stress concentrations. Local load sharing has been of most interest in recent times, starting with simplified two dimensional composites [40], i.e. tapes, and load sharing for three dimensional unidirectional fiber arrays have also been investigated [41, 42]. Batdorf, Bader, Priest, Harlow and Phoenix [39, 43, 44], compared these different load sharing mechanisms and how they affected the resulting composite strength. Smith, McCartney, Newman and Phoenix [45–47] incorporated time-dependent failure mechanisms. A detailed discussion and summary of applicable theory can be found in Phoenix and Beyerlein [37], and [48, 49] also provide an extensive review. For this type of composite, where the load is primarily carried by unidirectional continuous fibers, the Weibull distribution has been found to be effective in describing failure strength.

The Weibull distribution for ultimate tensile strength results from the starting assumption that the occurrence of natural, inherent flaws along a fiber is well described by a Poisson-Weibull model. The probability of failure for the basic two parameter Weibull distribution is given by [36]:

$$P_f = 1 - \exp \left\{ - \frac{L}{L_0} \left( \frac{\sigma}{\sigma_{\text{ref}}} \right)^\alpha \right\}, \quad (1)$$

where  $\sigma_{\text{ref}}$  is the Weibull scale parameter,  $\alpha$  is the Weibull shape parameter,  $L$  is the specimen length and  $L_0$  is a reference length.

Modeling of time-dependent properties of fibers was addressed by Phoenix and Newman [46, 47]. For the PPTA fibers in the UD laminate studied here, the rate dependence of the composite laminate is predominantly driven by the binder matrix properties as compared to PPTA fibers. At slow loading rates, the matrix has time to creep in shear, thus increasing the overloaded length next to a broken fiber. At slow loading rates, the matrix creep properties play a defining role in the composite's strength. In contrast, at fast loading rates, there is no time for the matrix to creep, so only the initial elastic overload length is relevant. This is described in detail in Engelbrecht-Wiggans [50].

### **Cunniff's strength to $V_{50}$ relation**

Cunniff described a relationship between a material's strength and the resulting armor's  $V_{50}$  [33]. He used dimensional analysis to determine a relationship between two dimensionless parameters, written in functional notation as:

$$\Phi \left( \Gamma_0, \frac{V_{50}}{\Omega^{1/3}} \right) = 0. \quad (2)$$

In (2), the first dimensionless parameter,  $\Gamma_0$ , is the ratio of the material's areal density to the projectile's sectional density:

$$\Gamma_0 = \frac{A_d A_p}{m_p}, \quad (3)$$

where  $A_d$  is the armor system areal density,  $A_p$  is the projectile presented area, and  $m_p$  is the projectile mass. The second dimensionless parameter in (2) is the  $V_{50}$  velocity scaled

by the cubed root of  $\Omega$ , where  $\Omega$  is the product of the material's specific toughness with the strain wave velocity:

$$\Omega = \frac{\sigma \varepsilon}{2\rho} \sqrt{\frac{E}{\rho}}, \quad (4)$$

where  $\sigma$  is the ultimate axial tensile stress,  $\varepsilon$  is the ultimate axial tensile strain,  $\rho$  is the material density, and  $E$  is the Young's modulus.

Ageing the material causes changes in its mechanical properties, including ultimate tensile stress, ultimate tensile strain, and Young's modulus. The material density is assumed to stay constant, as was seen in [17], where the linear density was unaffected by the sorption/desorption of water. The ratio of the  $V_{50}$  of aged material with that of unaged material, for a constant projectile type, can then be calculated as a function of these material parameters as follows. As the projectile type is fixed,  $\Gamma_0$  is constant. Since the relationship between the two terms in (2) is bijective, if the first term is constant then the second dimensionless term in (2) must also remain constant. Thus,  $V_{50}$  is proportional to the cubed root of  $\Omega$ :

$$V_{50} \propto \Omega^{1/3}. \quad (5)$$

Writing this for aged and unaged material gives the ratio

$$\begin{aligned} \frac{V_{50 \text{ aged}}}{V_{50 \text{ new}}} &= \left( \frac{\Omega_{\text{aged}}}{\Omega_{\text{new}}} \right)^{\frac{1}{3}} = \left( \frac{\sigma_{\text{aged}} \varepsilon_{\text{aged}}}{2\rho} \sqrt{\frac{E_{\text{aged}}}{\rho}} \frac{2\rho}{\sigma_{\text{new}} \varepsilon_{\text{new}}} \sqrt{\frac{\rho}{E_{\text{new}}}} \right)^{\frac{1}{3}} \\ &= \left( \frac{\sigma_{\text{aged}} \varepsilon_{\text{aged}}}{\sigma_{\text{new}} \varepsilon_{\text{new}}} \sqrt{\frac{E_{\text{aged}}}{E_{\text{new}}}} \right)^{\frac{1}{3}}. \end{aligned} \quad (6)$$

For these UD composite laminates, the stress-strain curve is typically linear, without a yielding region, such that

$$E = \frac{\sigma}{\varepsilon}. \quad (7)$$

Substituting (6) into (5) give the expression

$$\frac{V_{50 \text{ aged}}}{V_{50 \text{ new}}} = \left( \frac{\sigma_{\text{aged}} \varepsilon_{\text{aged}}}{\sigma_{\text{new}} \varepsilon_{\text{new}}} \sqrt{\frac{\sigma_{\text{aged}} \varepsilon_{\text{new}}}{\sigma_{\text{new}} \varepsilon_{\text{aged}}}} \right)^{\frac{1}{3}} = \left( \frac{\sigma_{\text{aged}}}{\sigma_{\text{new}}} \right)^{\frac{1}{2}} \left( \frac{\varepsilon_{\text{aged}}}{\varepsilon_{\text{new}}} \right)^{\frac{1}{6}}, \quad (8)$$

where the  $V_{50}$  retention of a material after ageing is a simple function of the aged and unaged ultimate tensile stress and strain.

### Phoenix- Porwal model's strength to $V_{50}$ relation

Cunniff derived (2) through (4) empirically from extensive data. Taking a theoretical approach, Phoenix and Porwal modeled ballistic impact into a homogeneous membrane

[34]. The resulting equation for  $V_{50}$  retention after ageing is notably similar to Cunniff's equation. Phoenix and Porwal derived that

$$V_{50} = \Omega^{\frac{1}{3}} \frac{2^{\frac{1}{3}} \varepsilon^{\frac{1}{12}} (1 + \theta^2 \Gamma_0)}{K_{\max}^{\frac{4}{3}}}, \quad (9)$$

where  $\Omega$  is the same as given in (4),  $\theta$  is an adjustment parameter, typically between 1.25 and 1.35, to account for various factors such as plastic projectile nose deformation, fabric wraparound, etc., and  $K_{\max}$  is given by:

$$K_{\max} = \exp \left\{ -\frac{4\theta^2 \Gamma_0 (\psi_{\max}^2 - 1)}{3(1 + \theta^2 \Gamma_0)} \right\} \psi_{\max}^{\frac{1}{2}} \left[ \frac{\sqrt{\frac{\psi_{\max}}{\varepsilon}} (\psi_{\max} - 1)}{\ln \left\{ 1 + \sqrt{\frac{\psi_{\max}}{\varepsilon}} (\psi_{\max} - 1) \right\}} \right]^{\frac{2}{3}}, \quad (10)$$

and where  $\psi_{\max}$  is approximated by

$$\psi_{\max} \approx \sqrt{\frac{1 + \theta^2 \Gamma_0}{2\theta^2 \Gamma_0}}. \quad (11)$$

The parameters  $\theta$  and  $\Gamma_0$  are projectile dependent, thus  $\theta$ ,  $\Gamma_0$ , and  $\psi_{\max}$  can be held constant such that

$$V_{50} \propto \Omega^{\frac{1}{3}} \varepsilon^{\frac{1}{12}} \left[ \frac{\ln \left\{ 1 + \sqrt{\frac{\psi_{\max}}{\varepsilon}} (\psi_{\max} - 1) \right\}}{\sqrt{\frac{\psi_{\max}}{\varepsilon}} (\psi_{\max} - 1)} \right]^{\frac{1}{2}}. \quad (12)$$

Thus,  $V_{50}$  retention is as follows, when using equations (9) through (11):

$$\begin{aligned}
\frac{V_{50 \text{ aged}}}{V_{50 \text{ new}}} &= \left( \frac{\Omega_{\text{aged}}}{\Omega_{\text{new}}} \right)^{\frac{1}{3}} \left( \frac{\varepsilon_{\text{aged}}}{\varepsilon_{\text{new}}} \right)^{\frac{1}{12}} \left( \frac{K_{\text{max new}}}{K_{\text{max aged}}} \right)^{\frac{3}{4}} \\
&= \left( \frac{\sigma_{\text{aged}}}{\sigma_{\text{new}}} \right)^{\frac{1}{2}} \left( \frac{\varepsilon_{\text{aged}}}{\varepsilon_{\text{new}}} \right)^{\frac{1}{6}} \left( \frac{\varepsilon_{\text{aged}}}{\varepsilon_{\text{new}}} \right)^{\frac{1}{12}} \left( \frac{\sqrt{\frac{\varepsilon_{\text{aged}}}{\varepsilon_{\text{new}}} \ln \left\{ 1 + \sqrt{\frac{\psi_{\text{max}}}{\varepsilon_{\text{aged}}} (\psi_{\text{max}} - 1)} \right\}}}{\sqrt{\frac{\varepsilon_{\text{aged}}}{\varepsilon_{\text{new}}} \ln \left\{ 1 + \sqrt{\frac{\psi_{\text{max}}}{\varepsilon_{\text{new}}} (\psi_{\text{max}} - 1)} \right\}}} \right)^{\frac{1}{2}} \\
&= \left( \frac{\sigma_{\text{aged}} \varepsilon_{\text{aged}}}{\sigma_{\text{new}} \varepsilon_{\text{new}}} \frac{\ln \left\{ 1 + \sqrt{\frac{\psi_{\text{max}}}{\varepsilon_{\text{aged}}} (\psi_{\text{max}} - 1)} \right\}}{\ln \left\{ 1 + \sqrt{\frac{\psi_{\text{max}}}{\varepsilon_{\text{new}}} (\psi_{\text{max}} - 1)} \right\}} \right)^{\frac{1}{2}} . \quad (13)
\end{aligned}$$

While more complicated than Cunniff's corresponding equation, (8), the two analyses give remarkably similar results. Furthermore, it can be shown that if  $\varepsilon_{\text{aged}} < \varepsilon_{\text{new}}$  then the  $V_{50}$  retention as predicted by Phoneix and Porwal, (13), will be more conservative, i.e. lower, than that predicted by Cunniff's equation, (8). A demonstration of this is given in the Appendix.

## Results

All data associated with this publication is archived through the NIST Public Data Repository at doi:10.18434/M32078 [51]. The UD material laminate was aged as described above for up to 150 d, with extractions made approximately every 30 d. Specimens were cut 30 mm wide at three different gauge lengths and tested at three different crosshead displacement rates. Figure 3 is a plot of the mean strength retention, i.e. the average ultimate tensile stress, also referred to as the strength, of at least 30 specimens divided by the initial average strength. The error bars in Figure 3 are the standard deviation of the mean strength retention divided by the square root of the number of specimens. Figure 4 is a plot of the Weibull scale parameter for the same specimens, where the error bars are the 95 % confidence interval from Maximum Likelihood Estimation. In both Figures 3 and 4 there is a general downward trend, indicative of degradation, although the percent degradation is less than 10 %, indicating that the material retains most of its strength after exposure to these ageing conditions. The numerical values for the specimens plotted in Figures 3 and 4 are given in Tables 1 through 3.

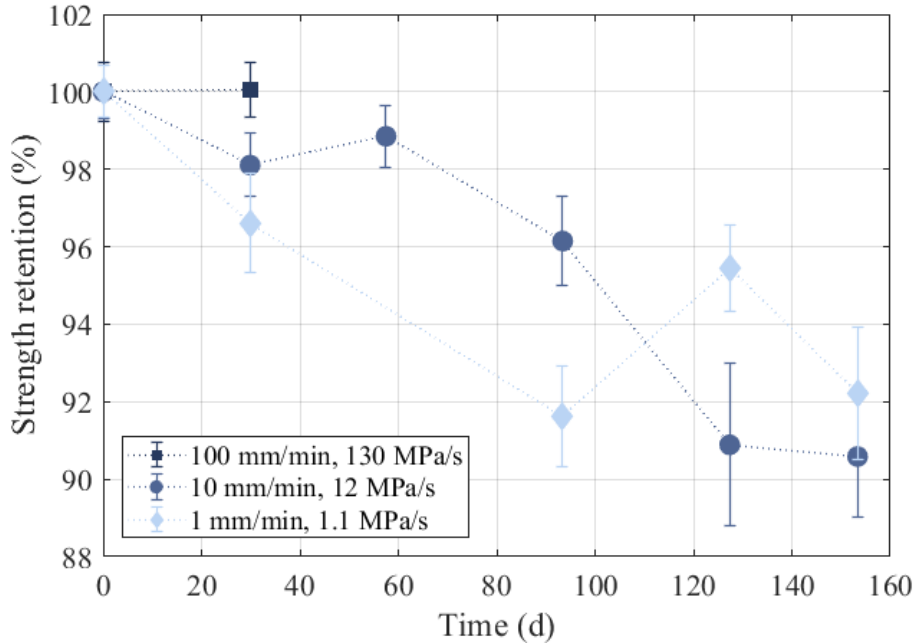


**Figure 3** Mean strength retention (%) as a function of days aged, where error bars represent approximately the standard error of the mean. Specimens are all 30 mm wide with a gauge length of 300 mm, tested at either 100 mm/min, 10 mm/min or 1 mm/min for the blue square, orange circle, and yellow diamond markers, respectively. Effective loading rates in terms of MPa/s are given in the legend.

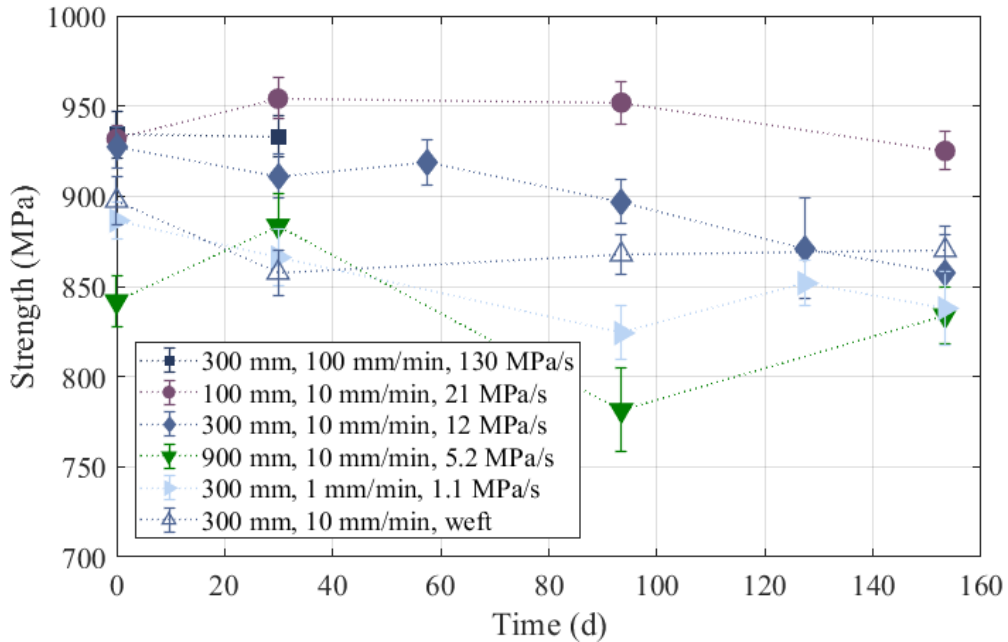


**Figure 4** Weibull strength scale parameters (MPa) as a function of ageing time (days), with the 95% confidence interval plotted as error bars. Specimens are all 30 mm wide, with varying gauge lengths and loading rates, as specified.

Tables 1 and Supplemental Table 1 give the mean values, with the standard deviations in parentheses, of each set of specimens for the ultimate tensile stress and ultimate tensile strain, respectively. Table 2 and Supplemental Table 2 give the Weibull scale and shape parameters of each set of specimens for the ultimate tensile stress and ultimate tensile strain, respectively. Table 3 and Supplemental Table 3 gives means, standard deviations, and Weibull scale and shape parameters for the weft specimens, cut at a gauge length of 300 mm and tested at a crosshead displacement rate of 10 mm/min, for ultimate tensile stress and strain, respectively. Each set consisted of between 27 and 44 specimens.

**Table 1** Mean ultimate tensile stress (MPa), with standard deviations in parentheses.

gauge (mm)	loading rate (mm/min)	days aged					
		0	30	58	93	127	153
300	1	872.2 (30.7)	859.1 (40.2)		816.9 (37.0)	840.9 (35.3)	821.5 (65.7)
300	10	908.6 (39.6)	899.1 (32.8)	898.2 (45.9)	892.6 (28.3)	851.4 (93.0)	837.6 (64.0)
300	100	913.3 (44.5)	914.5 (40.8)				
100	10	920.1 (25.3)	942.5 (30.1)		940.7 (29.4)		906.3 (36.2)
900	10	818.3 (51.6)	858.4 (58.7)		745.8 (86.1)		808.9 (56.0)

**Table 2** Weibull scale and shape (in parentheses) parameters for ultimate tensile stress (MPa).

gauge (mm)	loading rate (mm/min)	days aged					
		0	30	58	93	127	153
300	1	886.6 (29)	886.0 (20)		824.1 (18)	851.8 (23)	837.8 (14)
300	10	927.0 (27)	911.1 (24)	918.7 (24)	896.9 (24)	870.8 (11)	857.3 (14)
300	100	934.2 (24)	933.2 (28)				
100	10	931.9 (41)	954.1 (27)		951.9 (25)		925.1 (28)
900	10	841.7 (19)	883.6 (17)		781.4 (11)		833.8 (17)

**Table 3** Mean and standard deviation (in parentheses), and Weibull scale and shape (in parentheses) parameters for ultimate tensile stress (MPa) for weft specimens with a gauge of 300 mm and loading rate of 10 mm/min.

	days aged			
	0	30	93	153
Mean (SD)	876.6 (45)	840.4 (38)	850.3 (37)	847.3 (54)
scale (shape)	897.5 (22)	857.6 (27)	867.7 (26)	870.1 (20)

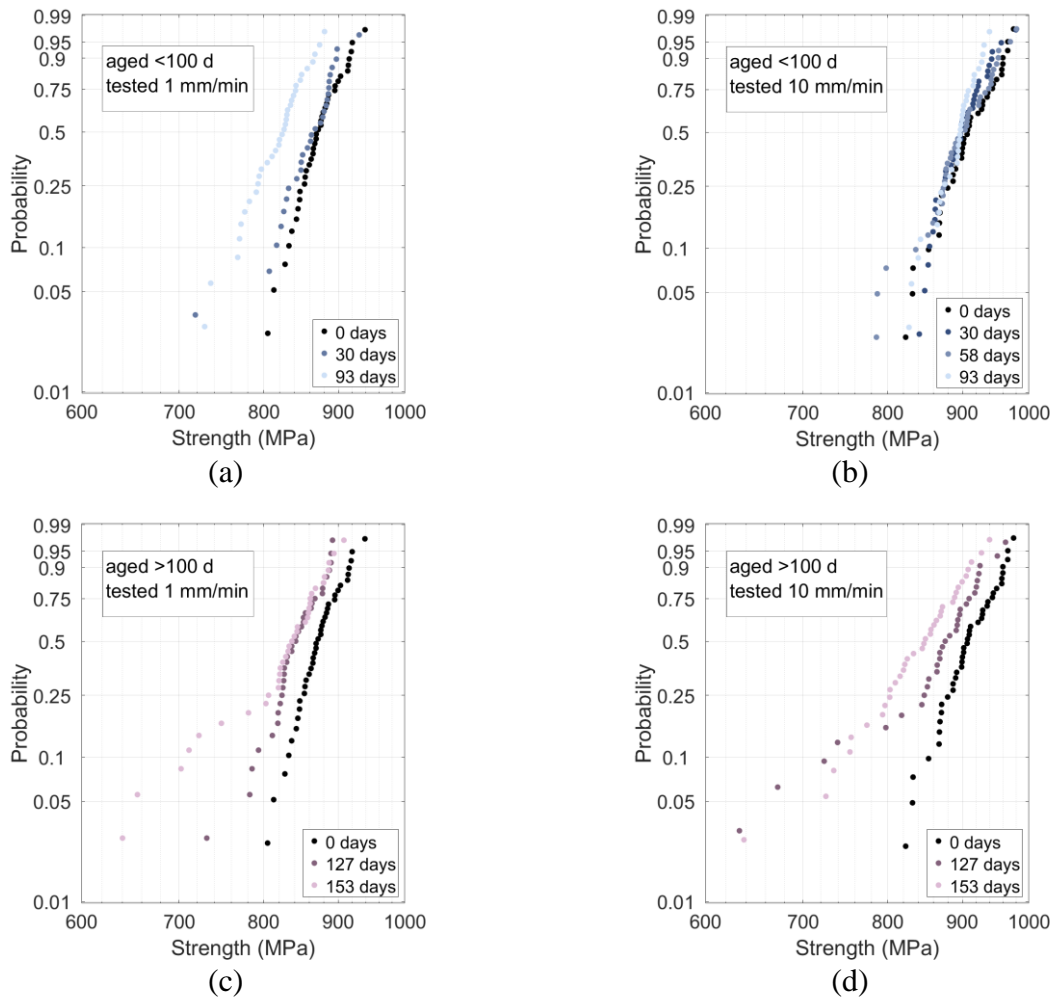


**Figure 5** Weibull probability plots of failure strength for specimens with a 300 mm gauge, (a) aged less than 100 d and tested at 1 mm/min, (b) aged less than 100 d and tested at 10 mm/min, (c) aged over 100 d and tested at 1 mm/min, and (d) aged over 100 d and tested at 10 mm/min.

Figure 5 is a collection of Weibull probability plots, comparing the failure distributions as a function of time for specimens aged less than 100 d (Figure 5a and 5b) and specimens

aged more than 100 d (Figure 5c and 5d). In Figure 5a and 5c, the specimens were tested at 1 mm/min and, in Figure 5b and 5d, the specimens were tested at 10 mm/min. During the first 100 d (Figures 5a and 5b), there is minimal to no degradation in the specimens tested at 10 mm/min (Figure 5b), in contrast to those tested at 1 mm/min (Figure 5a), where the curves shift left with ageing and barely overlap each other. The slight overlap that does occur may be due to the random sampling. After 100 d of ageing (Figures 5c and 5d), however, the specimens tested at 10 mm/min do start to degrade as demonstrated by the shift between the curves, while the specimens tested at 1 mm/min are more consistent above a strength of about 800 MPa. In both Figure 5c and Figure 5d, the lower tails of the aged distributions lengthen, increasing the overall variability. For the specimens tested at 10 mm/min, for the first 100 d the median of the distribution is fairly constant (less than 0.5% difference in the median), but after 100 d the median starts to shift left and the lower tails spread out. In contrast, for the specimens tested at 1 mm/min, the median starts to shift immediately, but stops after 100 d, when the lower tail spreads out.

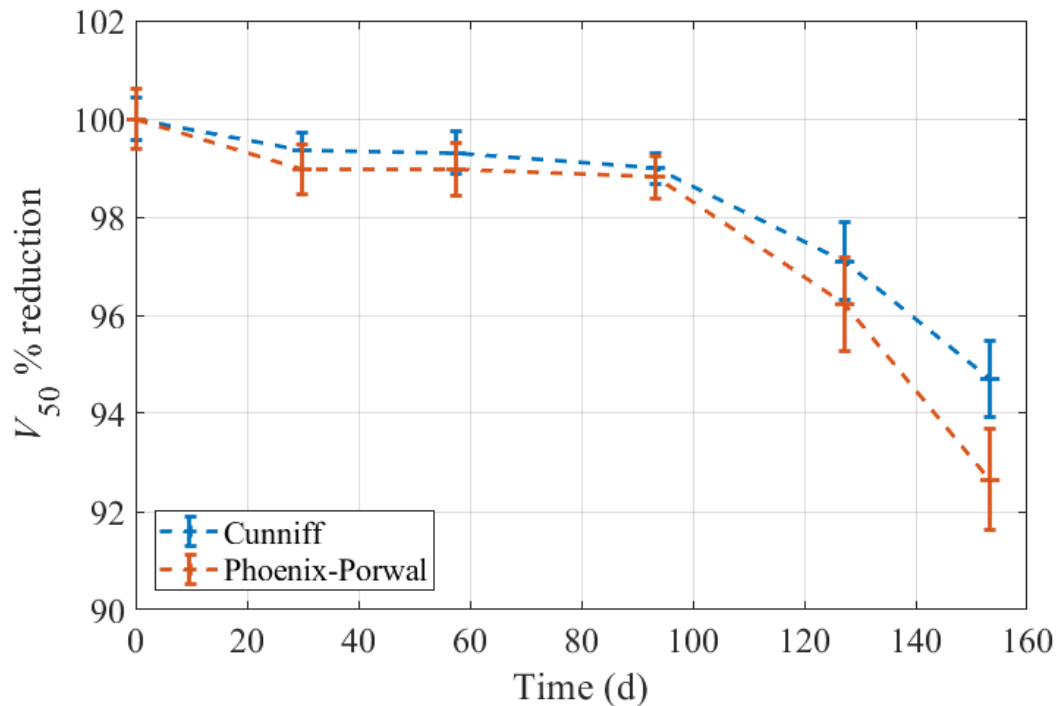


**Figure 6**  $V_{50}$  retention for the 300 mm gauge length specimens tested at a loading rate of 10 mm/min. Error bars represent the standard error of the mean, i.e. standard deviation divided by the square root of the number of samples.

Figure 6 shows the percent  $V_{50}$  retention for the specimens with a 300 mm gauge, tested at 10 mm/min, i.e. the same specimens as in Figure 5a. The  $V_{50}$  values were calculated for each specimen, using equation (4) and (12), with  $\psi = 1.6$  (although analysis has shown that  $V_{50}$  retention appears to be relatively insensitive to the value of  $\psi$ ). Then the results at each extraction time were averaged and divided by the mean from the initial unaged material in order to determine the mean  $V_{50}$  retention. The error bars in Figure 6 are the standard deviation of the calculated  $V_{50}$  retention divided by the square root of the number of samples. While the two models, Cunniff and Phoenix-Porwal, are very similar, the Phoenix-Porwal model consistently predicts a greater loss in  $V_{50}$ . Both models predict  $V_{50}$

retention of greater than 92 % for all specimens tested after 150 d at 70 °C and 76 % RH. The 900 mm specimens showed the greatest decrease in  $V_{50}$ , with the Cunniff model predicting 94 % and Phoenix-Porwal model predicting 92 % of the initial  $V_{50}$ . These values are very similar to the 150 d aged data presented in Figure 6.

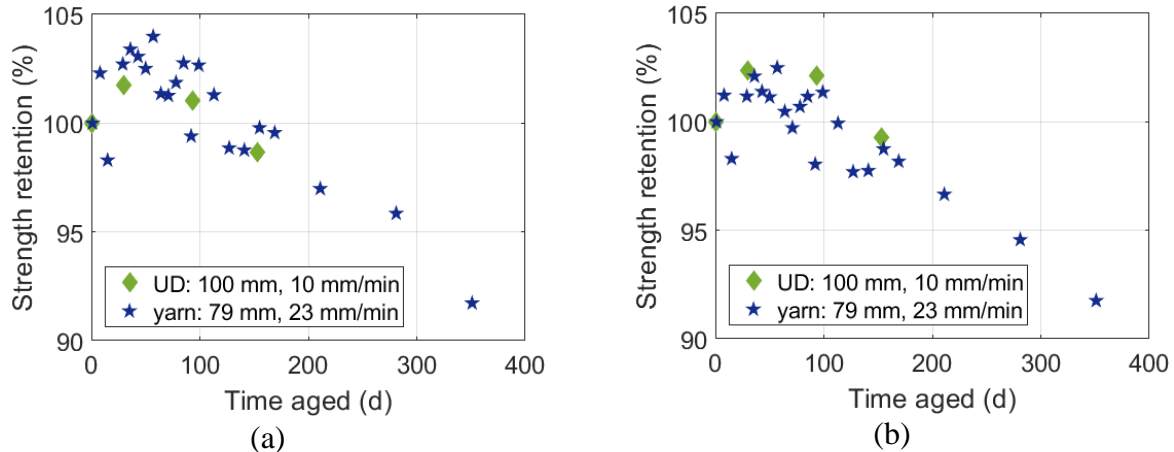


**Figure 7** Strength retention of the a) mean and b) Weibull scale parameter for PPTA UD laminate specimens with a 100 mm gauge length compared to PPTA yarn specimens with a gauge length of 79 mm, 1.6 twists per cm, tested at 23 mm/min, data from [7].

Figure 7 shows that the UD laminate specimens tested at the shortest gauge length are highly comparable to yarn specimens. The fibers in both the UD laminate and the yarns are PPTA, the gauge lengths are similar (100 mm and 79 mm), and the loading rates are also similar (10 mm/min and 23 mm/min).

## Discussion

Though a decrease in mechanical properties was observed as function of ageing time, a certain amount of scatter in the data from a single set of specimens is expected, due to the nature of the Weibull distribution that describes the ultimate strength. Each set of specimens tested herein consisted of between 27 and 44 specimens to provide relatively high confidence intervals on the mean and/or Weibull scale parameter. While a distribution of failure strengths is expected, there are other considerations that may further complicate comparisons between various datasets. In particular, the strength may exhibit variation within the roll. This could be due to damage, such as to the edges of the roll or the outermost layers, caused during manufacture or transportation and handling. Location-dependent strength may also be attributed to manufacturing defects. Manufacturing defects were observed in one location in the 20 meter long roll used, and that portion of the laminate was discarded. However, other manufacturing irregularities that cannot be visually detected may also exist that could lead to variability in the strength. Figure 8a and 8b show examples of macroscopic damage, while Figure 8c shows kink bands which are a potential smaller scale form of damage. When the roll of material was cut into strips for the ageing chambers, some randomization of the original roll location occurred within sets of specimens taken for testing. This randomization was minimal, so any location-dependence in strength would have been generally preserved. If there is no locational variation in strength, then the effect of randomizing specimen location would be nonexistent. With

randomization the strength distribution is widened, and assuming that the locational strength variation is caused by defects, randomization would decrease the average strength value. Location dependence will be considered for future studies but is not further investigated or discussed here.

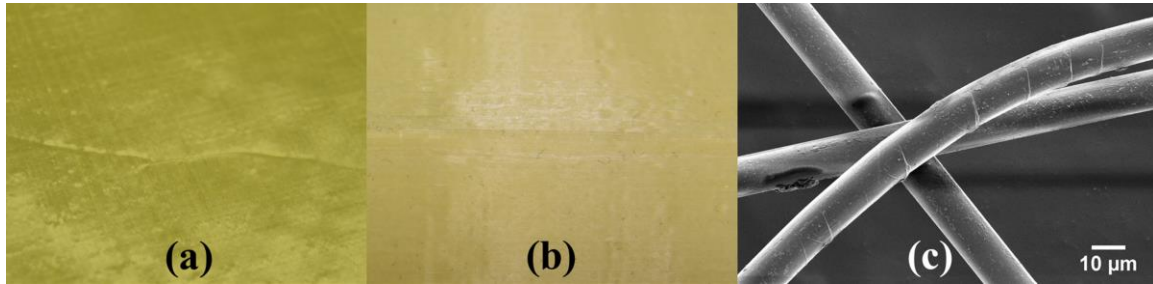


Figure 8 Images of damaged UD laminate material showing (a) visually detectable damage in the form of a fold (b) missing horizontal yarns and (c) single fiber kink bands, which cannot be discerned without a microscope.

Another consideration is the cutting accuracy with regards to a constant width specimen of exactly 30 mm wide. Specimens were nominally 30 mm wide, and the cutting method used ensured an average width of 30 mm, however, variations in width between individual specimens could be as much as 1 mm. The specimens with a gauge length of 900 mm were more challenging to cut. This resulted in more specimens damaged (and thus discarded) during the cutting process, resulting in fewer specimens per set, as well as more error in the effective width of these specimens. Despite precautionary measures in specimen preparation, some of the tested 900 mm gauge length specimens may have had other forms of damage along the cut edge that did not appear in the shorter specimens. Because of the difficulty in accurately cutting a 30 mm wide strip for a specimen with a gauge length of 900 mm, these specimens have considerably more variation in their strength (higher standard deviation, lower Weibull shape parameter) than the wider specimens.

Prior work [7] shows that the tensile strength of aramid yarns did not decrease before 100 d of exposure at the 70 °C and 76 % RH condition. In that study there is some evidence that, at 70 °C, there may be a superficial increase in aramid strength that lasts until the 100 d mark. This is potentially attributable to a change in the amount of friction at fiber surfaces, perhaps from sizing. The strength increase will be the subject of a future publication.

For the material and geometries we studied, the slowest loading rate reveals that most of the degradation occurs prior to 100 d of ageing, as seen in Figure 3. Since the degradation is more prominent in the slower loading rates in the first 100 d than it is for the higher loading rates in the same time period, this leads to the conclusion that there is degradation in the binder resin. In fact, in [35] we included an SEM image showing that the binder resin on the outside of the laminate is disappearing with ageing. After 100 d of ageing, the PPTA fibers may begin to degrade, which could potentially explain why the loading rate versus degradation trend does not continue after 100 d. The specimens tested at the slowest loading rates remain the weakest, even after 100 d, as can be seen in Figure 4. While the difference between the specimens that are unaged and those aged 153 d is typically on the order of one standard deviation, this difference is multiple standard errors, and the failure distributions are distinct, as shown in Figure 5 for the specimens with a gauge length of 300 mm, tested at 10 mm/min and 1 mm/min.

While the majority of the specimens had a gauge length of 300 mm, specimens with gauge lengths of 100 mm and 900 mm were also tested. The Weibull shape parameter should be independent of the volume of material, yet the opposite is seen in this data. The increased variation in the 900 mm specimens is directly attributable to the increased difficulty, and thus error, in preparing specimens for testing. When comparing the variation in 100 mm and 300 mm gauge specimens, the variability is initially unaffected by ageing. The final ageing interval for the 100 mm specimens has variability consistent with the previous 100 mm specimen data, while the variability increases for the 300 m specimens after 100 d. Maximum likelihood 95 % confidence intervals for the scale parameter can be seen in Figure 3, and 95 % confidence intervals for the shape parameter would be larger, given the population of approximately 30 specimens.

The appearance of failed specimens differs as a function of gauge length, but not of ageing or of loading rate. At 100 mm, practically none of the specimens had fully separated by the time the load had declined 90 % from the ultimate load. In contrast, most of the 300 mm specimens, and all of the 900 mm specimens, fully separated into two pieces during failure. Furthermore, the 900 mm specimens become wrinkled during failure.

In comparing the warp direction specimens to the weft direction specimens, the weft direction specimens are initially weaker than the warp specimens, perhaps due to extra handling of the weft fibers in manufacturing. The material degradation was thus more evident in the warp direction specimens (as seen in Figure 3), though after 150 d at 70 °C and 76 % RH, their strengths were comparable.

At most, the degradation in strength for any of the specimens is less than 10 % of the initial strength and was observed mostly in the specimens tested at slower loading rates. Obviously, these specimens were all tested well below the speed of a ballistic event. Using Cunniff and Phoenix-Porwal's  $V_{50}$  predictions, the level of degradation observed in these tests would predict a reduction of less than 8% in the predicted  $V_{50}$  for the Cunniff or the Phoenix-Porwal models. Based on other research [22], there is reason to believe that these predictions may be conservative, and that the true reduction in  $V_{50}$  may be even less than that predicted by the Cunniff or the Phoenix-Porwal models. However, the observed variance is small enough that there does appear to be discernable degradation, even though it is fairly small.

## **Conclusions and Future Work**

The strength of the PPTA flexible UD laminate specimens we studied degrades with exposure, however, the degradation in ultimate tensile stress is less than 10 % after 150 d at 70 °C and 76 % RH. Since these PPTA UD laminate samples were exposed to accelerated ageing conditions, this result of minimal degradation is encouraging for the use of this material as a real-world body armor material, where the degradation environment would be much less harsh. This observation is underscored by a predicted reduction in the  $V_{50}$  of armor made from this material of only 8 %. During the first 100 d of accelerated ageing, degradation seems to mainly occur in the binder resins. Strength degradation in the PPTA fibers begins after 100 d exposure.

Future work should pinpoint the causes of the observed degradation in failure strength, including examining the chemical composition of the fibers, binder and interface for

changes with ageing; determining the effects of additional ageing, both environmental but also including mechanical damage such as folding and abrasion; examining the binder resin using different techniques; and establishing whether binder degradation alone leads to reduced  $V_{50}$  performance, with or without delamination of the composite.

## Acknowledgements

The authors would like to acknowledge Dr. Michael Riley for his assistance in conducting the experiments, and Vivian Yu and Shefei Jiang for assistance with testing.

## Conflicts of Interest

The authors declare that they have no conflicts of interest in presenting this work. Funding for Engelbrecht-Wiggans was provided under grant NIST 70NANB17H337. Funding for Forster was provided from the Department of Defense through interagency agreement R17-643-0013.

## Appendix

### Comparison of Cunniff and Phoenix-Porwal approaches to empirically-determined ballistic limit

In comparing equations (8) and (13), it can be shown that the two equations differ by the term:

$$\left( \frac{\varepsilon_{\text{aged}}}{\varepsilon_{\text{new}}} \right)^{\frac{1}{3}} \left[ \frac{\ln \left\{ \left[ 1 + \sqrt{\frac{\psi}{\varepsilon_{\text{aged}}}} (\psi - 1) \right]^{\sqrt{p}} \right\}}{\ln \left\{ 1 + \sqrt{\frac{\psi}{\varepsilon_{\text{new}}}} (\psi - 1) \right\}} \right]^{\frac{1}{2}}. \quad (14)$$

It can be shown that if the strain after ageing is less than the strain before ageing then the Phoenix-Porwal model will always predict a greater change in  $V_{50}$  than is predicted by the Cunniff model. A demonstration follows.

Bernoulli's equation states that if  $r \in [0,1]$  and  $x \geq -1$ , then

$$(1+x)^r \leq 1+rx. \quad (15)$$

Define

$$p \equiv \frac{\varepsilon_{\text{aged}}}{\varepsilon_{\text{new}}}, \quad (16)$$

and assume

$$\begin{aligned}
0 < p &\leq 1 \\
\psi &> 1 \\
\varepsilon_{\text{new}} &> 0
\end{aligned} \tag{17}$$

Then

$$\sqrt{p} \in [0,1], (\psi - 1) > 0, \sqrt{\psi} > 1, \frac{1}{p} \geq 1 \text{ and } \frac{1}{\varepsilon_{\text{new}}} > 0, \tag{18}$$

such that

$$\sqrt{\frac{\psi}{p\varepsilon_{\text{new}}}}(\psi - 1) > 0 \geq -1. \tag{19}$$

Using (15), then

$$\begin{aligned}
\left[1 + \sqrt{\frac{\psi}{p\varepsilon_{\text{new}}}}(\psi - 1)\right]^{\sqrt{p}} &\leq 1 + \sqrt{p} \sqrt{\frac{\psi}{p\varepsilon_{\text{new}}}}(\psi - 1) \\
\left[1 + \sqrt{\frac{\psi}{p\varepsilon_{\text{new}}}}(\psi - 1)\right]^{\sqrt{p}} &\leq 1 + \sqrt{\frac{\psi}{\varepsilon_{\text{new}}}}(\psi - 1)
\end{aligned} \tag{20}$$

so

$$\ln \left\{ \left[1 + \sqrt{\frac{\psi}{p\varepsilon_{\text{new}}}}(\psi - 1)\right]^{\sqrt{p}} \right\} \leq \ln \left\{ 1 + \sqrt{\frac{\psi}{\varepsilon_{\text{new}}}}(\psi - 1) \right\}, \tag{21}$$

where

$$\ln \left\{ \left[ \sqrt{\frac{\psi}{p\varepsilon_{\text{new}}}}(\psi - 1) \right]^{\sqrt{p}} \right\} = \sqrt{p} \ln \left\{ \sqrt{\frac{\psi}{p\varepsilon_{\text{new}}}}(\psi - 1) \right\}. \tag{22}$$

Since  $p^{\frac{2}{3}} \leq p^{\frac{1}{2}}$ , (21) becomes

$$\begin{aligned}
p^{\frac{2}{3}} \ln \left\{ \left[1 + \sqrt{\frac{\psi}{p\varepsilon_{\text{new}}}}(\psi - 1)\right]^{\sqrt{p}} \right\} &\leq p^{\frac{1}{2}} \ln \left\{ \left[1 + \sqrt{\frac{\psi}{p\varepsilon_{\text{new}}}}(\psi - 1)\right]^{\sqrt{p}} \right\} \\
&\leq \ln \left\{ 1 + \sqrt{\frac{\psi}{\varepsilon_{\text{new}}}}(\psi - 1) \right\}
\end{aligned} \tag{23}$$

The term  $\ln \left\{ 1 + \sqrt{\frac{\psi}{\varepsilon_{\text{new}}}}(\psi - 1) \right\}$  is positive as  $1 + \sqrt{\frac{\psi}{\varepsilon_{\text{new}}}}(\psi - 1) > 1$ , so

$$\frac{p^{\frac{2}{3}} \ln \left\{ \left[ 1 + \sqrt{\frac{\psi}{p\epsilon_{\text{new}}}} (\psi - 1) \right]^{\sqrt{p}} \right\}}{\ln \left\{ 1 + \sqrt{\frac{\psi}{\epsilon_{\text{new}}}} (\psi - 1) \right\}} \leq 1. \quad (24)$$

Thus

$$p^{\frac{1}{3}} \left[ \frac{\ln \left\{ \left[ 1 + \sqrt{\frac{\psi}{p\epsilon_{\text{new}}}} (\psi - 1) \right]^{\sqrt{p}} \right\}}{\ln \left\{ 1 + \sqrt{\frac{\psi}{\epsilon_{\text{new}}}} (\psi - 1) \right\}} \right]^{\frac{1}{2}} \leq 1, \quad (25)$$

Or

$$\left( \frac{\epsilon_{\text{aged}}}{\epsilon_{\text{new}}} \right)^{\frac{1}{3}} \left[ \frac{\ln \left\{ \left[ 1 + \sqrt{\frac{\psi}{\epsilon_{\text{aged}}}} (\psi - 1) \right]^{\sqrt{p}} \right\}}{\ln \left\{ 1 + \sqrt{\frac{\psi}{\epsilon_{\text{new}}}} (\psi - 1) \right\}} \right]^{\frac{1}{2}} \leq 1, \quad (26)$$

which is the difference between the Cunniff model's and the Phoenix-Porwal model's predictions for the reduction in  $V_{50}$ .

## Supplemental

**Supplemental Table 1** Mean ultimate tensile strain (%), with standard deviations in parentheses

gauge (mm)	loading rate (mm/min)	days aged					
		0	30	58	93	127	153
300	1	2.72 (0.09)	2.77 (0.07)		2.61 (0.12)	2.64 (0.10)	2.63 (0.17)
300	10	2.79 (0.12)	2.76 (0.10)	2.76 (0.08)	2.78 (0.08)	2.71 (0.11)	2.57 (0.18)
300	100	2.67 (0.13)	2.70 (0.12)				
100	10	2.86 (0.09)	2.86 (0.09)		2.92 (0.08)		2.88 (0.12)
900	10	2.57 (0.13)	2.56 (0.15)		2.36 (0.24)		2.47 (0.15)

**Supplemental Table 2** Weibull scale and shape (in parentheses) parameters for ultimate tensile strain (%)

gauge (mm)	loading rate (mm/min)	days aged					
		0	30	58	93	127	153
300	1	2.76 (32)	2.78 (27)		2.65 (23)	2.68 (28)	2.68 (20)
300	10	2.85 (29)	2.79 (27)	2.80 (38)	2.80 (26)	2.76 (15)	2.63 (15)
300	100	2.74 (24)	2.76 (26)				
100	10	2.90 (38)	2.89 (31)		2.93 (27)		2.92 (25)
900	10	2.62 (25)	2.62 (20)		2.46 (12)		2.52 (21)

**Supplemental Table 3** Mean and standard deviation (in parentheses), and Weibull scale and shape (in parentheses) parameters for ultimate tensile strain (%) for weft specimens with a gauge of 300 mm and loading rate of 10 mm/min

	days aged			
	0	30	93	153
Mean (SD)	2.80 (0.12)	2.71 (0.11)	2.71 (0.13)	2.68 (0.14)
scale (shape)	2.86 (31)	2.76 (31)	2.77 (24)	2.74 (24)

### Fiber Volume Fraction Determination

The following procedure was used to estimate the fiber volume fraction from the SEM micrographs:

1. Estimation of average fiber cross-sectional area: Three SEM micrographs were obtained using similar magnification settings, and then contrast corrected. Fiber surfaces with clearly defined cross-sections (not damaged from the cutting process) were used for determining fiber cross-sectional area. Approximately 3 to 4 individual fibers were carefully selected from each micrograph and a freeform boundary was manually constructed using a commercially available image processing software. Finally, the area enclosed within the boundary was estimated, as shown below. Statistical outlier values of individual fiber surface area were eliminated as determined by 1.5 times the inter-quartile range.

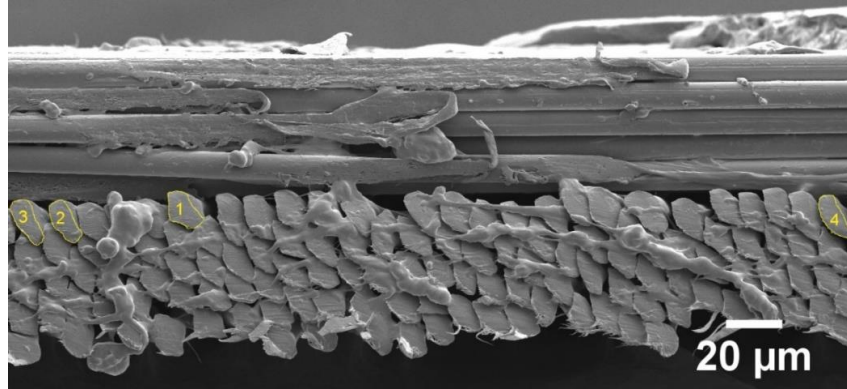


**Figure S1** SEM micrograph of a cross section of a UD laminate with the indicated highlighted areas used to estimate the cross-sectional area of different fibers.

2. Next, a rectangular region was chosen from four SEM micrographs and the total number of fibers within the identified region was manually determined.
3. Using the individual fiber cross sectional area, and the estimate of the total number of fibers per unit area, an approximate fiber volume fraction was estimated as shown in the table below.

**Supplemental Table 4** Calculations for the estimation of net fiber volume fraction in a UD laminate. The standard deviations are derived from at least three measurements for SEM cross-section area ( $Area_{SEM}$ ), fibers within the SEM cross-section area ( $N_{fiber}$ ), and the average fiber cross-section area ( $Area_{fiber}$ ).

	<b>Area SEM (<math>\mu m^2</math>)</b>	<b><math>N_{fiber}</math></b>	<b>Area<sub>fiber</sub> (<math>\mu m^2</math>)</b>	<b>Area<sub>total</sub> (<math>\mu m^2</math>) Area<sub>fiber</sub> x <math>N_{fiber}</math></b>	<b>Fiber Fraction (%) (Area<sub>total</sub>/Area<sub>SEM</sub>) x 100</b>
<b>Average</b>	16865.8	133.8	99.5	13306.4	78.9
<b>Std. dev</b>	244.8	4.8	2.4	571.4	3.6

## References

1. IACP/DUPONT™ KEVLAR® SURVIVORS' CLUB®. <http://www.dupont.com/products-and-services/personal-protective-equipment/body-armor/articles/the-kevlar-survivors-club.html>. Accessed 17 Jan 2017
2. Chin J, Forster A, Clerici C, et al (2007) Temperature and humidity aging of poly(p-phenylene-2,6-benzobisoxazole) fibers: Chemical and physical characterization. *Polym Degrad Stab* 92:1234–1246. <https://doi.org/10.1016/j.polymdegradstab.2007.03.030>
3. Forster AL, Pintus P, Messin GHR, et al (2011) Hydrolytic stability of

- polybenzobisoxazole and polyterephthalamide body armor. *Polym Degrad Stab* 96:247–254. <https://doi.org/10.1016/j.polymdegradstab.2010.10.004>
4. National Institute of Justice (2008) Ballistic Resistance of Body Armor. U.S. Department of Justice, Office of Justice Programs, Washington, DC
  5. Forster AL, Forster AM, Chin JW, et al (2015) Long-term stability of UHMWPE fibers. *Polym Degrad Stab* 114:45–51. <https://doi.org/10.1016/j.polymdegradstab.2015.01.028>
  6. Tsinas Z, Forster AL, Al-Sheikhly M (2018) Oxidation reactions in kink banded regions of UHMMPE fiber-based laminates used in body armor: A mechanistic study. *Polym Degrad Stab* 154:103–114. <https://doi.org/10.1016/j.polymdegradstab.2018.05.030>
  7. Rice KD, Engelbrecht-Wiggans AE, Guigues E, Forster AL (2018) Evaluation of Degradation Models for High Strength p-Aramid Fibres Used in Body Armour. In: Proceedings of the Personal Armour Systems Symposium. Washington, DC
  8. Park AD (1999) United States Patent Ballistic Laminate Structure in Sheet Form Patent Number : 5935678
  9. Mourtiz AP (2012) Manufacturing of fibre–polymer composite materials. In: Introduction to Aerospace Materials. Woodhead Publishing, pp 303–337
  10. Springer H, Obaid AABU, Prabawa AB, Hinrichsen G (1998) Influence of Hydrolytic and Chemical Treatment on the Mechanical Properties of Aramid and Copolyaramid Fibers. *Text Res J* 68:588–594
  11. Auerbach I (1989) Kinetics for the tensile strength degradation of Nylon and Kevlar yarns. *J Appl Polym Sci* 37:2213–2227. <https://doi.org/10.1002/app.1989.070370813>
  12. Morgan R, Butler N (1992) Hydrolytic degradation mechanism of kevlar 49 fibers when dissolved in sulfuric acid. *Polym Bull* 27:689–696
  13. Derombise G, Vouyovitch Van Schoors L, Klop EA, et al (2012) Crystallite size evolution of aramid fibres aged in alkaline environments. *J Mater Sci* 47:2492–2500. <https://doi.org/10.1007/s10853-011-6073-8>
  14. Arrieta C, David É, Dolez P, Vu-Khanh T (2011) Hydrolytic and photochemical aging studies of a Kevlar-PBI blend. *Polym Degrad Stab* 96:1411–1419. <https://doi.org/10.1016/j.polymdegradstab.2011.05.015>
  15. Derombise G, Van Schoors LV, Davies P (2010) Degradation of Aramid Fibers Under Alkaline and Neutral Conditions: Relations Between the Chemical Characteristics and Mechanical Properties. *J Appl Polym Sci* 116:2504–2514
  16. Guangming C, Haihua Y, Weidong W (2008) Evaluation of light and thermal aging performance of aramid fabric. In: Textile Bioengineering and Informatics Symposium Proceedings. pp 321–325
  17. Obaid AA, Deitzel JM, Gillespie JW, Zheng JQ (2011) The effects of environmental conditioning on tensile properties of high performance aramid fibers at near-ambient

- temperatures. *J Compos Mater* 45:1217–1231
18. Zhang H, Zhang J, Chen J, et al (2006) Effects of solar UV irradiation on the tensile properties and structure of PPTA fiber. *Polym Degrad Stab* 91:2761–2767
  19. Bourbigot S, Flambard X, Poutch F (2001) Study of the thermal degradation of high performance fibres - Application to polybenzazole and p-aramid fibres. *Polym Degrad Stab* 74:283–290. [https://doi.org/10.1016/S0141-3910\(01\)00159-8](https://doi.org/10.1016/S0141-3910(01)00159-8)
  20. Obaid AA, Yarlagadda S, Gillespie JW (2016) Combined effects of kink bands and hygrothermal conditioning on tensile strength of polyarylate liquid crystal copolymer and aramid fibers. *J Compos Mater* 50:339–350. <https://doi.org/10.1177/0021998315574754>
  21. Chin J, Byrd E, Clerici C, et al (2007) Chemical and Physical Characterization of Poly (p-phenylene-2,6-benzobisoxazole) Fibers Used in Body Armor: Temperature and Humidity Aging. NISTIR 7373
  22. Forster AL (2012) Long Term Stability and Implications for Performance of High Strength Fibers Used in Body Armor. University of Maryland, College Park
  23. ASTM E3110-18 Standard Test Method for Collection of Ballistic Limit Data for Ballistic-resistant Torso Body Armor and Shoot Packs
  24. Koh CP, Shim VPW, Tan VBC, Tan BL (2008) Response of a high-strength flexible laminate to dynamic tension. *Int J Impact Eng* 35:559–568. <https://doi.org/10.1016/j.cancergen.2015.03.013>
  25. Russell BP, Karthikeyan K, Deshpande VS, Fleck NA (2013) The high strain rate response of Ultra High Molecular-weight Polyethylene: From fibre to laminate. *Int J Impact Eng* 60:1–9. <https://doi.org/10.1016/j.ijimpeng.2013.03.010>
  26. Czechowski L, Jankowski J, Kubiak T (2012) Experimental tests of a property of composite material assigned for ballistic products. *Fibres Text East Eur* 92:61–66
  27. Levi-Sasson A, Mustacchi S, Amarilio I, et al (2014) Experimental determination of linear and nonlinear mechanical properties of laminated soft composite material system. *Compos Part B Eng* 57:96–104
  28. Chen L, Zheng K, Fang Q (2017) Effect of strain rate on the dynamic tensile behaviour of UHMWPE fibre laminates. *Polym Test* 63:54–64. <https://doi.org/10.1016/j.polymertesting.2017.07.031>
  29. Mittelman A, Roman I (1991) Monitoring the tensile deformation in real unidirectional Kevlar-epoxy composites. *NDT&E Int* 24:85–89. [https://doi.org/10.1016/0963-8695\(91\)90822-K](https://doi.org/10.1016/0963-8695(91)90822-K)
  30. Marais C, Feillard P (1992) Manufacturing and mechanical characterization of unidirectional composites. *Compos Sci Technol* 45:247–255
  31. Chocron Benloulo IS, Rodríguez J, Martínez MA, Sánchez Gálvez V (1997) Dynamic tensile testing of aramid and polyethylene fiber composites. *Int J Impact Eng* 19:135–146. [https://doi.org/10.1016/S0734-743X\(96\)00017-6](https://doi.org/10.1016/S0734-743X(96)00017-6)
  32. Rodriguez J, Chocron Benloulo IS, Martinez MA, Sanchez-Galvez V (1996) High

- strain rate properties of aramid and polyethylene woven fabric composites. *Compos Part B Eng* 27:147–154
33. Cunniff PM (1999) Dimensionless Parameters for Optimization of Textile-Based Armor Systems. In: 18th International Symposium on Ballistics. San Antonio, TX, pp 1302–1310
  34. Phoenix S, Porwal P (2003) A new membrane model for the ballistic impact response and V50 performance fo multi-ply fibrous systems. *Int J Solids Struct* 40:6723–6765
  35. Engelbrecht-Wiggans AE, Krishnamurthy A, Burni F, et al (2019) Cutting Procedures, Tensile Testing, and Ageing of Flexible Unidirectional Composite Laminates. *J Vis Exp* in press:
  36. Weibull W (1951) A Statistical Distribution Function of Wide applicability. *J Appl Mech* 18:293–297
  37. Phoenix SL, Beyerlein IJ (2000) Statistical Strength Theory for Fibrous Composite Materials. In: Kelly A, Zweben C (eds) *Comprehensive Composite Materials*. Elsevier, pp 559–639
  38. Daniels HE (1945) The statistical theory of the strength of bundles of threads. I. *Proc R Soc London Ser A Math Phys Sci* 183:405–435. <https://doi.org/10.1098/rspa.1945.0011>
  39. Batdorf SB (1982) Tensile Strength of Unidirectionally Reinforced Composites- I. *J Reinf Plast Compos* 1:153–164
  40. Zweben C, Rosen BW (1970) A statistical theory of material strength with application to composite materials. *J Mech Phys Solids* 18:189–206. [https://doi.org/10.1016/0022-5096\(70\)90023-2](https://doi.org/10.1016/0022-5096(70)90023-2)
  41. Hedgepeth, M. J (1961) Stress Concentrations in Filamentary Structures
  42. Hedgepeth JM, Van Dyke P (1967) Local Stress Concentrations in Imperfect Filamentary Composite Materials. *J Compos Mater* 1:294–309. <https://doi.org/10.1177/002199836700100305>
  43. Bader MG, Priest AM (1982) Statistical aspects of fibre and bundle strength in hybrid composites. In: Hayashi T, Kawata S, Umekawa S (eds) *Progress in Science and Engineering Composites, ICCM-IV*. pp 1129–1136
  44. Harlow DG, Phoenix SL (1978) The Chain-of-Bundles Probability Model for the Strength of Fibrous Materials II: A Numerical Study of Convergence. *J Compos Mater* 12:314–334. <https://doi.org/10.1177/002199837801200308>
  45. McCartney LN, Smith RL (1983) Statistical Theory of the Strength of Fiber Bundles. *J Appl Mech* 105:601
  46. Newman WI, Phoenix SL (2001) Time-dependent fiber bundles with local load sharing. *Phys Rev E - Stat Nonlinear, Soft Matter Phys* 63:20. <https://doi.org/10.1103/PhysRevE.63.021507>
  47. Phoenix SL, Newman WI (2009) Time-dependent fiber bundles with local load

sharing. II. General Weibull fibers. *Phys Rev E - Stat Nonlinear, Soft Matter Phys* 80:1–14. <https://doi.org/10.1103/PhysRevE.80.066115>

48. Sutherland LS, Soares CG (1997) Review of probabilistic models of the strength of composite materials. *Reliab Eng Syst Saf* 56:183–196. [https://doi.org/10.1016/S0951-8320\(97\)00027-6](https://doi.org/10.1016/S0951-8320(97)00027-6)
49. Mishnaevsky L, Brøndsted P (2009) Micromechanical modeling of damage and fracture of unidirectional fiber reinforced composites: A review. *Comput Mater Sci* 44:1351–1359. <https://doi.org/10.1016/j.commat.2008.09.004>
50. Engelbrecht-Wiggans AE (2017) Analysis and Test Strategies for Stress Rupture in Unidirectional Continuous Fiber Composite Structures. Ph.D. Dissertation, Cornell University
51. Engelbrecht-Wiggans A, Forster AL (2019) Data Publication: Aged and unaged flexible unidirectional composite laminate tensile testing for soft body armor applications